RSC Advances

ROYAL SOCIETY OF CHEMISTRY

www.rsc.org/advances

Mechanically Reinforced Composite Aerogel blocks by Self-growing Nanofibers †‡

Xibin Yi,[*a,b] Linlin Zhang,[a,c] Fengyun Wang,[*d] Xiaodong Shen,[b] Sheng Cui,[b] Jing Zhang[a] and Xiuchun Wang[a]

Received (in XXX, XXX) Xth XXXXXXXXX 20XX, Accepted Xth XXXXXXXXX 20XX
DOI: 10.1039/b000000x

Here we report the preparation of mechanically reinforced composite aerogels using self-growing nanofibers. This approach was used to grow ZrO_X nanofibers with chemical imbalance in SiO_2 precursor solution and establish the property–structure relationship between mechanical properties and self-growing nanofibers of ZrO_x/SiO_2 aerogels. As-synthesized ZrO_x/SiO_2 aerogels show high compressive strength (9.68 MPa) and high BET surface area (827.22 $m^2 \cdot g^{-1}$). These novel ZrO_x/SiO_2 aerogels could be used as thermal isolates.

Aerogel material is a sort of porous solid in which the air percolates through the network of SiO_2 nanoparticles.[1, 2] It is typically synthesized with sol–gel method and generally obtained by supercritical drying.[3, 4] Due to its excellent properties,[5] such as porosity,[6] low density,[7] high surface area[7] and low thermal conductivity,[2] aerogel material has been widely applied to different kinds of fields.[8-14] However, the machining ability and application of aerogel material are greatly limited by its fragility.[1, 15] Therefore, improving the mechanical properties and insulation performance of aerogels[16-18] have become the main direction and long-term goals for the research of modern insulation materials.[19-21]

Recent research has proven that the addition of inorganic fibers into aerogel blocks is an effective way to reinforce its mechanical properties, which has become the hot spot research.[17, 19, 20, 22-25] According to the literatures, the strength of aerogel skeleton could be enhanced by the addition of thin skeleton solid particles,[26, 27] or the inorganic/organic fiber.[27-30] However, it should be noted that the apparently enhanced strength does not mean the frangibility is improved,[23, 31] and also the radiation heat transfer[22] and the heat conduction are reduced.[22, 24, 31, 32] In other words, the addition of inorganic micron-fibers material cannot improve the strength of aerogel blocks[33]. The main reason is that various reinforced fibers can improve the mechanical properties of aerogel, however, the reinforcing fibers cannot match the structures of aerogels.[24, 31, 32] As a result, it could lead to the formation of capillary tension in the bonding interface between the fibers and aerogel, which may result in structural cracking or even collapsing under the high temperature. However, in sol-gel process, synchronously synthesizing reinforced fibers[25, 34, 35] and aerogel can effectively improve the performance between the fibers and the aerogel. Zhong[34] et al have fabricated the alumina nanofiber reinforced composite aerogels(C/Al_2O_3) with high compressive strength (5.4–9.1 MPa) and Young's modulus (286.95–476.71 MPa).

Several studies have demonstrated that adding nanomaterials has played a better supporting role than the addition of micron-fibers material in promoting high-temperature stability and structure of SiO_2 aerogels.[6, 25, 32] Although various reinforcing fibers can improve the mechanical properties of the aerogels, their diameters are larger than nano-scale structures of the aerogels, which will cause the increase of capillary tension in the adhesive bonding interface of the aerogel. Moreover, structure cracking or collapsing would easily occur due to large residual stress formed by poor interfacial bonding between aerogels and fibers. These structure cracking or collapsing aerogels could not be used as thermal isolates. The problem of poor performance combined with the fibers and the aerogels can be effectively solved by synchronous synthesizing the self-growing fibers and the nanomaterials in the sol-gel process.

Based on our research, it can be deduced that the optimal method to obtain reinforced aerogel blocks is self-growing nanofibers in sol-gel process, in which the density and the specific surface area of the aerogel blocks would not significantly increase. At the same time, the thermal insulators and the fragility could also be improved. In this paper, we report the preparation of mechanically reinforced aerogel blocks depending on acid-based imbalance theory in the precursor solution of SiO_2 aerogels (Scheme 1), which the atom aggregating would happen to grow well-defined ZrO_x nanofibers on the Zr^{4+} ions surface. The block composite xerogels can be prepared by supercritical drying after gel-aging, following which the composite aerogel blocks can be obtained by heat treatment. It can be observed in the later test that there is a property–structure correlation between the molar mass of nanofibers and the mechanical reinforcement of the aerogel blocks.

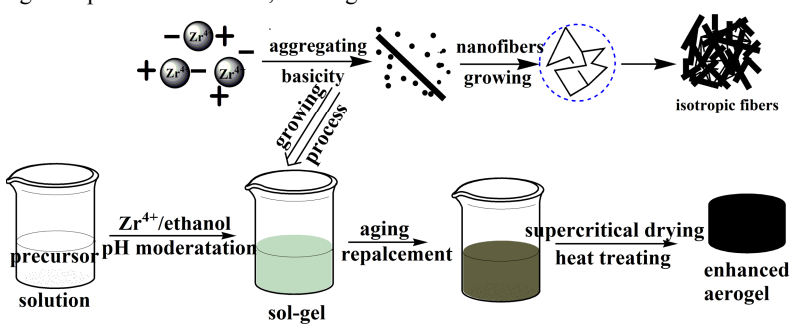

Scheme1 Synthesis route of ZrO_x/SiO_2 aerogels

In this paper, ZrO_X/SiO_2 composite aerogels reinforced by self-growing nano-fibers are prepared. In the sol-gel process, supercritical drying technology and high-temperature heat treatment are required. We use tetraethylorthosilicate (TEOS) as the silicon source, trimethylchlorosilane (TMCS) as the modifier, crystalline salts $ZrCl_4$ as the zirconium source, anhydrous sodium carbonate (Na_2CO_3) as the reaction catalyst, deionized water (H_2O) and anhydrous ethanol (C_2H_5OH) as the solvent. After heat treatment at 1200 ºC, the specific surface area of the composited aerogel achieves to value 827.22 $m^2 \cdot g^{-1}$, the compressive strength is up to 9.68 MPa and the true density is 0.23 $g \cdot cm^{-3}$. This result is mainly because that the zirconium oxide has good heat resistance, whose disorder intersperse can effectively improve the mechanical properties and the high temperature stability of SiO_2 aerogels.

Self-growing nano-fibers are conducted in solution by acid-based imbalance on the Zr^{4+} ions surface. And this chemical imbalance causes an increasing of the mechanical tension in the surface of particles, which causes the movement of nanoparticles. When two particles attract each other, the imbalance ends and dehydration reaction emerges. Depending on the dissolved-growth mechanism, the small particles grow gradually in the radial direction. After thermostatic aging for 24 h, granular particles would disappear, and the product would present a fibrous morphology.

After heat treatment, the porous network structure of the overall composite aerogels does not change, and the nanofibers remain in SiO_2 aerogels. Compared with pure SiO_2 aerogels or the SiO_2 composite aerogels (reinforced by the addition of micron-fibers material), ZrO_X/SiO_2 composite aerogel shows completely different characteristic and advantage, and especially the mechanical property is improved significantly after the addition of self-growing nanofibers.

After supercritical drying and heat treatment, the composite aerogel becomes a complete massive sample without obvious cracks on the surface as shown in Fig. 1A, which is feasible to prepare high-strength composite aerogel blocks. Fig. 1B is a scanning electron microscopy (SEM) image, which shows the microstructure of the composite aerogel surface similar to aerogel materials before high temperature heat treatment.[1, 36] The disordered porous nanostructure shows a typical "pearl chain" of crosslinked and high porosity skeleton network. Fig. 1C and 1D respectively show transmission electron microscopy (TEM) images of the composite aerogel before and after heat treatment. An alkaline environment is conducive to the formation of nanofibers in aerogel aging process.[34] The existence of nanofiber helps to improve mechanical properties of the composite aerogel, and zirconium oxide nanofibers have excellent heat resistance, which have no cracking by 1200 °C heat treatment (Fig. 1D).

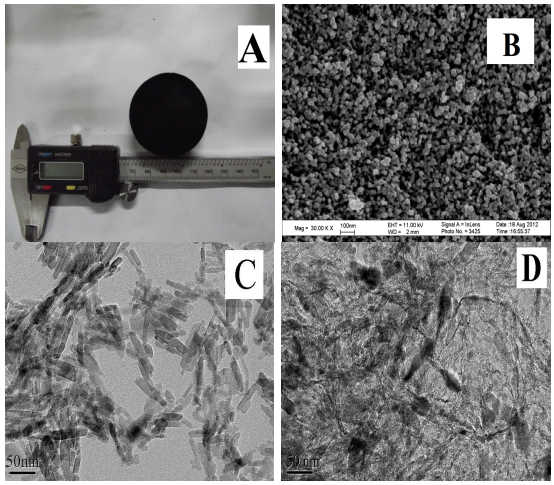

Fig. 1 real photos (A) and the SEM (B), TEM(C, D) of the ZrO_X/SiO_2 aerogel

Fig. 2 shows the XRD spectra of the composite aerogels before and after heat treatment. The dried aerogel before heat treatment is a typical amorphous substance as shown in Fig. 2A. After heat treatment at 1200 °C, the amorphous form (shown in Fig. 2B) of SiO_2 composite aerogel remains, and the $ZrSiO_4/ZrO_2$ "mixed crystal" phase appears mostly, and ZrO_2 diffraction peak is significantly higher than $ZrSiO_4$ diffraction peak. Wherein 2θ diffraction peaks of 27.8°, 31.2°, 48.7° and 65.1° correspond to positions of {111}, {200}, {221}, and {131} planes of ZrO_2 (PDF No 72-597, Fig. 2C), respectively, 2θ diffraction peaks of 26.8°, 35.4°, 53.2° and 67.8° correspond to the positions of {220}, {311}, {400} and {440} of the crystal plane $ZrSiO_4$ (PDF No.3-443, Fig. 2D), respectively. The XRD patterns of the composite aerogels indicate that the compositions of the nanofibers are ZrO_2 (mainly) and $ZrSiO_4$. $ZrSiO_4$ would not be formed in the lower temperature. With temperature rising, ZrO_2 migrates to the surface and the surface reaction of Si-O compound would occur which lead to the formation of $ZrSiO_4$. $ZrSiO_4$ diffraction peaks indicate that the nanofibers (Fig. 1D) and the surrounding SiO_2 particles are connected together by chemical bonds, and this method is essentially different from the physical-reinforce method of adding fibers into the aerogels. XRD spectra also show that the disorderly distribution of these nanofibers has played a key role in increasing the strength of aerogel.

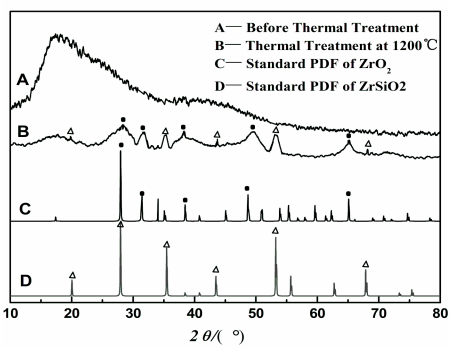

Fig.2 XRD patters of aerogels before & after heat treatment

After the heat treatment of the composite aerogel, the chemical attribute of resulting aerogels was analyzed by X-ray

photoelectron spectroscopy (XPS). Figure 3 shows the O1s XPS spectra of the aerogel. The pollution carbon (electron binding energy of 285.0 eV) was used as the internal standard to obtain the electron binding energy of oxygen peak curve. According to the results shown in Fig. 2, the chemical bonds of the composited aerogel are respectively O-Si bond, O-Zr bond and Si-O-Zr bond. Corresponding to the XPS analysis in Fig. 3, the electron binding energy of the O1s is 531.58 eV, O-Si bond corresponding electron binding energy is 532.08 eV, O-Zr bond is 532.55 eV, and Si-O-Zr bond is 533.28 eV. The three O elements contents (atomic %) of the binding energy of oxygen are 73.91 eV for O-Si bond, 16.33 eV for O-Zr bond, and 9.86 eV for Si-O-Zr bond, respectively, which means that the removal of the free O-O binding energy happened.

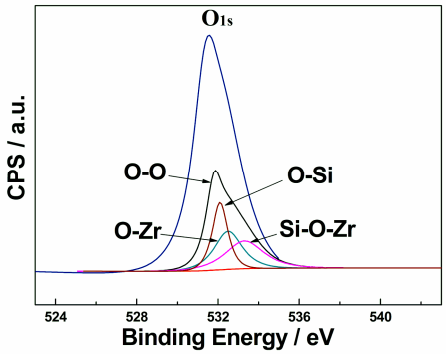

Fig.3 XPS patters of aerogels before & after heat treatment

Thermogravimetric analysis (TGA) was carried out to determine the chemical composition of the aerogel (as shown in Fig. 4). The global analysis reveals that aerogel lose its weight in two stages. Assuming that the weight loss before 100 °C is mainly associated to the adsorbed water and the volatized ethanol on the aerogel surface, the ratio is 15.9%. Weight loss between 590 °C to 855.3 °C is mainly associated to the dehydration of some ligand by the non-bridging hydroxyl groups or the bridging hydroxyl groups, the dehydration of zirconium oxide hydrate, and the aerogel surface remaining Si-OH condensation caused by dehydration, the ratio is 2.47%. There is a weak exothermic peak intensity at 850 °C, which indicates the zirconia phase transition from amorphous to crystalline. After 855.3 °C, the curve tends to be smooth. It means that the aerogel composition and the structure went stable.

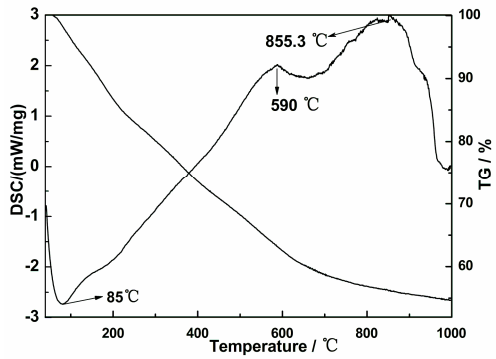

Fig.4 TG-DSC curve of the composte aerogel

The specific surface areas and pore structure characteristics have been further evaluated by nitrogen adsorption/desorption technique. The relevant data are summarized in Table 1. In addition, the pore size distribution curves and adsorption/desorption isotherms of aerogels samples are shown in Fig. 5. The adsorption/desorption isotherms of the aerogels before (Fig. 5A) and after (Fig. 5B) thermal treatment are typical Type IV curves according to the IUPAC classification, suggesting that they are typical mesoporous materials. All of the aerogels samples before and after thermal treatment have high BET (Brunauer–Emmett–Teller) surface area, as indicated by the change in volume of adsorbed N_2. Before the heat treatment, the ZrO_x aerogels sample (Fig.5A) had high adsorption capacity and large mesoporous pore, which makes the surface area reach to 642.83 $m^2 \cdot g^{-1}$. From the pore size distribution, it can be seen that the composite aerogels after thermal treatment show a broad pore size distribution from 2 nm to 50 nm, the surface area of 827.22 $m^2 \cdot g^{-1}$. The corresponding average pore size decreases from 200 nm (before the thermal treatment) to 40.23 nm (after the thermal treatment) because of the stretching action and the contraction.[34, 36]Before the thermal treatment, the microscopic network structure was not stable enough. As a result, the number of large pores reduced during the increase of the temperature of thermal treatment, which results in the decrease of the amount of adsorption. After the heat treatment, the internal structures of SiO_2 aerogel particles and zirconium oxide particles became stable, where there were no shrinkage and cracks shown in Fig. 1D. The framework of composite aerogels was more stable, and the pores sizes were well-distributed in the specific scope, as suggested by the SEM images (Fig. 1B).

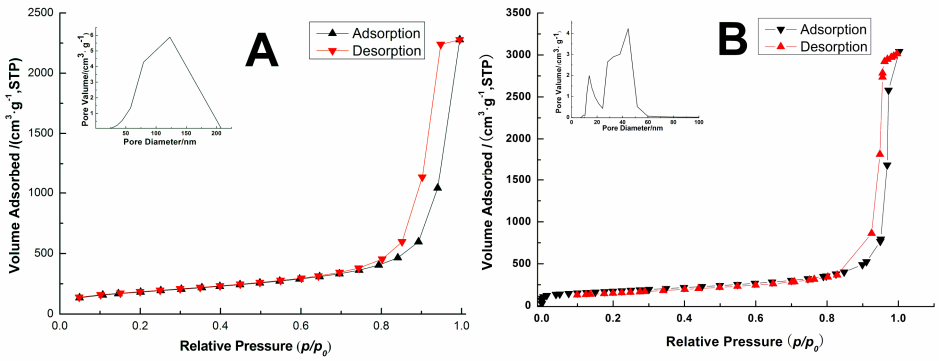

Fig.5 N_2 adsorption/desorption isotherms and pore-size of aerogels before (A) and after (B) heat treatment

Table 1 the micro-structural parameters and mechanical properties of the aerogels before and after heat treatment

Heat treatment[a]	Density[b] /g·cm^{-3}	Compressive strength/MPa	BET/ m^2·g^{-1}	Pore volume /cm^3·g^{-1}
Before	0.17	1.74	642.83	5.88
After	0.23	9.68	827.22	4.34

[a] Select the excellent same sample. [b] Measured by AccuPyc II 1340 Density Analyzer.

Table 2 physical properties of the reported aerogels with comparative block density.

Sample	Block density/g·cm^{-3}	Compressive Young's modulus/MPa	Reference
Al_2O_3	0.181	11.4	37
Carbon	0.1-0.3	10-200	38
SiO_2	0.180	3.88	39
TiO_2	0.193	3.5	40
$C_{2\text{-}50}/SiO_2$	0.15-0.21	23-52	41
Layer/SiO_2	0.288	8.77	42
C-Al_2O_3	0.184	9.1	34

As can be seen from Table 1, the specific surface area of ZrO_x/SiO_2 aerogels after heat treatment significantly achieves to value 827.22m^2·g^{-1}. The removal of the residual organic groups, the shrinkage of the pore structure between the particles, and the evaporation of water molecules in the high temperature processing could increase in the number of mesopores. Zirconium oxides still exist in the form of nanofibers after the heat treatment, and the presence of the nanofibers could be confirmed from TEM images. The presence of this form is also important to maintain the high specific surface area of the composite aerogel. Furthermore, during the heat treatment, the partial destruction of pore structure occurred, so that the density increased to 0.23 g·cm^{-3}. Table 1 also shows that the compressive strength increased significantly after heat treatment. The main reason is that there are shrinkages between particles of the pore structure during heat treatment, so the reinforcement of skeleton network structure appeared. At the same time, the existence of the zirconium oxide nanofibers makes the endurance of aerogel structure increase, for which the final compressive strength is up to 9.68 MPa. The compressive strength of ZrO_x/SiO_2 aerogels has a distinct advantage compared to the known research data (inorganic aerogels which can be used in high temperature) in Table 2.

In this paper, the monolith high strength ZrO_X/SiO_2 composite aerogel was prepared with crystalline zirconium chloride, tetraethyl orthosilicate, trimethylchlorosilane, and ethanol, the sol-gel method combined with CO_2 supercritical drying, and the high temperature heat treatment. Such amorphous aerogels were used as a versatile precursor to synthesize zirconium oxides with diverse valences and crystallographic phases. After heat treatment at 1200 °C, the as-synthesized monolith ZrO_X/SiO_2 aerogels had a interpenetrating network structure, and the compressive strength of ZrO_X/SiO_2 aerogel was 9.68 MPa without the use of other structural reinforcement materials, the specific surface area was 827.22 m^2·g^{-1} and the density was 0.23 g·cm^{-3}. The analysis shows that the zirconium oxide nanofibers self-grown in the precursor solution of aerogel in the sol-gel process and the aging process. The self-growing nanofibers interpenetrated in the internal network structure, and connected to the SiO_2 particles with the chemical bond, so the aerogel skeleton was reinforced, and the compressive strength was significantly increased. This method was completely different from the conventional way of adding-fiber reinforced aerogel. And because of the presence of zirconium oxide nanofibers, the heat resistance temperature of the ZrO_X/SiO_2 aerogel reached to 1200 °C effectively. Therefore, the outstanding mechanical behavior and high-temperature resistance of the novel porous ZrO_X/SiO_2 material offers a broad scope of application prospects in the field of aeronautical, satellite, vessel high temperature protection, etc. In addition, the preparation method also provides a new design idea for the reinforcement of aerogel.

Acknowledgment

This work is supported by the National Nature Science Foundation of China (51402176, 51402160), the Young and Middle-Aged Scientists Research Awards Fund of Shandong Province (BS2013CL038), the Science and Technology Development Plan Project of Shandong Province (2013YD02046), the Youth Fund Projects of Shandong Academy of Sciences (2013QN019) and the Open Project of the State Key Laboratory of Materials-Oriented Chemical Engineering (KL12-07).

Notes and references

[a] *Institute of the New Material Research, Shandong Academy of Sciences, Key Laboratory for Adhesion & Sealing Materials of Shandong Province, Jinan 250014, P. R. China. Fax & Tel: +86 531 8872 8308; E-mail: yixb@sdas.org*

[b] *College of Materials Science and Technology, State Key Laboratory of Materials-Oriented Chemical Engineering, Nanjing University of Technology, Nanjing 210009, P. R. China*

[c] *School of Materials Science and Engineering, Shandong Jianzhu University, Jinan 250101,China*

[d] *The Cultivation Base for State Key Laboratory, Qingdao University. Qingdao 266071, P. R. China. Tel: +86 532 83780318; E-mail: fywang@qdu.edu.cn*

† Electronic Supplementary Information (ESI) available: Materials, preparation and characterisation of ZrO_X/SiO_2 composite aerogel. See DOI: 10.1039/b000000x/.

‡ The first and second corresponding authors contributed equally to this research.

1. A. Tadjarodi, M. Haghverdi and V. Mohammadi, *Materials Research Bulletin*, 2012, **47**, 2584-2589.
2. T. Xie, Y.-L. He and Z.-J. Hu, *International Journal of Heat and Mass Transfer*, 2013, **58**, 540-552.
3. K. Nawaz, S. J. Schmidt and A. M. Jacobi, *International Journal of Heat and Mass Transfer*, 2014, **74**, 25-34.
4. K. S. Morley, P. Licence, P. C. Marr, J. R. Hyde, P. D. Brown, R. Mokaya, Y. Xia and S. M. Howdle, *Journal of Materials Chemistry*, 2004, **14**, 1212-1217.

5. A. Neugebauer, K. Chen, A. Tang, A. Allgeier, L. R. Glicksman and L. J. Gibson, *Energy and Buildings*, 2014, **79**, 47-57.
6. Y. Tang, K. L. Yeo, Y. Chen, L. W. Yap, W. Xiong and W. Cheng, *Journal of Materials Chemistry A*, 2013, **1**, 6723-6726.
7. J. Li, J. Li, H. Meng, S. Xie, B. Zhang, L. Li, H. Ma, J. Zhang and M. Yu, *Journal of Materials Chemistry A*, 2014, **2**, 2934-2941.
8. P. Li, J. Li, Q. Zhu, L. Cui and H. Li, *RSC Advances*, 2013, **3**, 8939-8946.
9. X. vv Liu, J. Cui, J. Sun and X. Zhang, *RSC Advances*, 2014, **4**, 22601-22605.
10. Z. Li, Y. Ji, C. Cadigan and R. M. Richards, *Catalysis Science & Technology*, 2014.
11. Z. Juanjuan, L. Ruiyi, L. Zaijun, L. Junkang, G. Zhiguo and W. Guangli, *Nanoscale*, 2014, **6**, 5458-5466.
12. S. Cui, W. Cheng, X. Shen, M. Fan, A. Russell, Z. Wu and X. Yi, *Energy & Environmental Science*, 2011, **4**, 2070-2074.
13. J. Liang, Z. Cai, L. Li, L. Guo and J. Geng, *RSC Advances*, 2014, **4**, 4843-4847.
14. S. Yun, H. Luo and Y. Gao, *RSC Advances*, 2014, **4**, 4535-4542.
15. Y. Kong, X. Shen, S. Cui and M. Fan, *Ceramics International*, 2014, **40**, 8265-8271.
16. L. Wang, M. Sánchez-Soto and M. L. Maspoch, *Materials & Design*, 2013, **52**, 609-614.
17. C.-Q. Hong, J.-C. Han, X.-H. Zhang and J.-C. Du, *Scripta Materialia*, 2013, **68**, 599-602.
18. M. Zhang, B. Gao, X. Cao and L. Yang, *RSC Advances*, 2013, **3**, 21099-21105.
19. F. Sabri, J. Marchetta and K. M. Smith, *Acta Astronautica*, 2013, **91**, 173-179.
20. A. E. Donius, A. Liu, L. A. Berglund and U. G. K. Wegst, *Journal of the Mechanical Behavior of Biomedical Materials*, 2014, **37**, 88-99.
21. Z. Han, Z. Tang, P. Li, G. Yang, Q. Zheng and J. Yang, *Nanoscale*, 2013, **5**, 5462-5467.
22. J.-J. Zhao, Y.-Y. Duan, X.-D. Wang and B.-X. Wang, *Journal of Non-Crystalline Solids*, 2012, **358**, 1303-1312.
23. X. Yang, Y. Sun and D. Shi, *Journal of Non-Crystalline Solids*, 2012, **358**, 519-524.
24. B. Yuan, S. Ding, D. Wang, G. Wang and H. Li, *Materials Letters*, 2012, **75**, 204-206.
25. W.-C. Li, A.-H. Lu, C. Weidenthaler, R. Goddard, H.-J. Bongard and F. Schuth, *Journal of Materials Chemistry*, 2005, **15**, 2993-2996.
26. P. D. Brown, S. K. Gill and L. J. Hope-Weeks, *Journal of Materials Chemistry*, 2011, **21**, 4204-4208.
27. J. Guo, B. N. Nguyen, L. Li, M. A. B. Meador, D. A. Scheiman and M. Cakmak, *Journal of Materials Chemistry A*, 2013, **1**, 7211-7221.
28. D. J. Boday, P. Y. Keng, B. Muriithi, J. Pyun and D. A. Loy, *Journal of Materials Chemistry*, 2010, **20**, 6863-6865.
29. A. Ricci, L. Bernardi, C. Gioia, S. Vierucci, M. Robitzer and F. Quignard, *Chemical Communications*, 2010, **46**, 6288-6290.
30. A. S. Wu, T.-W. Chou, J. W. Gillespie, D. Lashmore and J. Rioux, *Journal of Materials Chemistry*, 2012, **22**, 6792-6798.
31. X. Yang, J. Wei, D. Shi, Y. Sun, S. Lv, J. Feng and Y. Jiang, *Materials Science and Engineering: A*, 2014, **609**, 125-130.
32. J. Feng, C. Zhang and J. Feng, *Materials Letters*, 2012, **67**, 266-268.
33. D. Shi, Y. Sun, J. Feng, X. Yang, S. Han, C. Mi, Y. Jiang and H. Qi, *Materials Science and Engineering: A*, 2013, **585**, 25-31.
34. Y. Zhong, Y. Kong, X. Shen, S. Cui, X. Yi and J. Zhang, *Microporous and Mesoporous Materials*, 2013, **172**, 182-189.
35. Z. Zhou, X. Zhang, C. Lu, L. Lan and G. Yuan, *RSC Advances*, 2014, **4**, 8966-8972.
36. Y. Kong, Y. Zhong, X. Shen, S. Cui, M. Yang, K. Teng and J. Zhang, *Journal of Non-Crystalline Solids*, 2012, **358**, 3150-3155.
37. G. Zu, J. Shen, X. Wei, X. Ni, Z. Zhang, J. Wang and G. Liu, *Journal of Non-Crystalline Solids*, 2011, **357**, 2903-2906.
38. R. W. Pekala, C. T. Alviso and J. D. LeMay, *Journal of Non-Crystalline Solids*, 1990, **125**, 67-75.
39. A. H. Alaoui, T. Woignier, G. W. Scherer and J. Phalippou, *Journal of Non-Crystalline Solids*, 2008, **354**, 4556-4561.
40. M. A. Worsley, S. O. Kucheyev, J. D. Kuntz, T. Y. Olson, T. Y.-J. Han, A. V. Hamza, J. H. Satcher and T. F. Baumann, *Chemistry of Materials*, 2011, **23**, 3054-3061.
41. M. Moner-Girona, E. Martínez, A. Roig, J. Esteve and E. Molins, *Journal of Non-Crystalline Solids*, 2001, **285**, 244-250.
42. K. A. D. Obrey, K. V. Wilson and D. A. Loy, *Journal of Non-Crystalline Solids*, 2011, **357**, 3435-3441.